AIAA JOURNAL
Vol. 41, No. 5, May 2003

Soot Surface Growth in Laminar Hydrocarbon/Air Diffusion Flames

A. M. El-Leathy,* F. Xu,† C. H. Kim,‡ and G. M. Faeth§
University of Michigan, Ann Arbor, Michigan 48109

The structure and soot surface growth properties of round, laminar, jet diffusion flames were studied experimentally. Measurements were made along the axes of ethylene-, propylene-, propane-, and acetylene–benzene-fueled flames burning in coflowing air at atmospheric pressure with the reactants at normal temperature. The measurements included soot structure, soot concentrations, soot temperatures, major gas species concentrations, some radial species (H, OH, and O) concentrations, and gas velocities. The results suggested that soot surface growth involved decomposition of the original fuel to form acetylene and H, which were the main reactants for soot surface growth, and that the main effect of the parent fuel on soot surface growth involved its yield of acetylene and H for present test conditions. Measurements of soot surface growth rates (corrected for soot surface oxidation) in laminar jet diffusion flames were consistent with earlier measurements of soot surface growth rates in laminar premixed flames and exhibited good agreement with existing hydrogen-abstraction/carbon-addition soot surface growth mechanisms in the literature with steric factors in these mechanisms having values on the order of unity, as anticipated.

Nomenclature

d_p	=	mean primary soot particle diameter, m
f_s	=	soot volume fraction
$[i]$	=	concentration of species i, kgmol $\cdot$ m^{-3}
R_i	=	terms in the hydrogen-abstraction/carbon-addition (HACA) soot surface growth rate formulas, kg $\cdot$ m^{-2} s^{-1}
T	=	temperature, K
u	=	streamwise velocity, ms^{-1}
w_g	=	soot surface growth rate, kg $\cdot$ m^{-2}s^{-1}
z	=	streamwise distance, m
α_i	=	empirical (steric) factors in the HACA soot surface growth rate formulas
ν	=	kinematic viscosity, m^{2}s^{-1}
ϕ	=	fuel-equivalence ratio

Subscripts

CH	=	HACA soot surface growth mechanism of Colket and Hall[17]
FW	=	HACA soot surface growth mechanism of Frenklach and Wang[18,19] and Kazakov et al.[20]

Introduction

SOOT is a major unsolved combustion problem because it is present in most hydrocarbon-fueled nonpremixed (diffusion) flames, and current understanding of soot processes in flame environments is limited. This lack of understanding inhibits progress toward developing reliable methods of computational combustion, predictions of pollutant soot emission properties, and estimates of flame radiation properties, among others. Motivated by these observations, the present investigation sought to extend earlier studies of soot processes in laminar premixed and diffusion flames completed in this laboratory,[1–8] using similar methods. The specific objectives of the present investigation were to obtain new experimental information about the structure and soot surface growth properties of hydrocarbon-fueled laminar jet diffusion flames burning in air at atmospheric pressure with the reactants at normal temperature and to exploit these results to evaluate contemporary models of soot surface growth properties in flame environments. The following description of the research is brief; more details and a complete tabulation of the measurements are provided by Xu[9] and El-Leathy.[10]

Earlier studies of the structure and soot surface reaction properties of laminar flames have been reviewed by Haynes and Wagner,[11] Howard,[12] Richter and Howard,[13] and Kennedy.[14] Therefore, present considerations of earlier work will be brief and will emphasize past studies in this laboratory that have motivated the objectives and methods of the present investigation. Sunderland et al.,[1] Sunderland and Faeth,[2] and Lin et al.[3] experimentally studied the structure and soot surface growth properties of laminar hydrocarbon-fueled (acetylene, ethane, propane, n-butane, propylene, and 1,3-butadiene) diffusion flames burning in air at pressures of 10–100 kPa; however, they were not able to evaluate available mechanisms of soot surface growth because their measurements did not provide information about H concentrations needed by the theories. Xu et al.[4,5] and Xu and Faeth[6] subsequently completed experimental investigations of the structure and soot surface growth properties of laminar premixed flames at atmospheric pressure including ethylene/air mixtures similar to the flames studied by Harris and Weiner[15] and methane/oxygen mixtures similar to the flames studied by Ramer et al.[16] Concentrations of H were found during these studies so that the measurements could be used to evaluate the hydrogen-abstraction/carbon-addition (HACA) soot surface growth mechanisms of Colket and Hall,[17] Frenklach and Wang,[18,19] and Kazakov et al.[20] It was found that the HACA soot surface growth mechanisms provided excellent correlations of the measurements using quite reasonable values of unknown empirical steric factors that appear in the theories. Xu and Faeth[7] extended study of soot surface growth from premixed flames to acetylene-fueled laminar jet diffusion flames burning in air at atmospheric pressure, using the full suite of measurements developed during the laminar premixed flame studies in Refs. 4–6. These results showed that soot surface growth rates in laminar premixed and diffusion flames satisfied similar reaction rate expressions and that these expressions were well represented by the HACA mechanisms of Colket and Hall,[17] Frenklach and Wang,[18,19] and Kazakov et al.[20] Finally, Xu et al.[8]

Received 5 August 2002; revision received 15 October 2002; accepted for publication 13 November 2002.

*Research Associate, Department of Aerospace Engineering.
†Research Associate, Department of Aerospace Engineering; currently Assistant Professor, Department of Mechanical, Materials, and Aerospace Engineering, University of Central Florida, Orlando, FL 32816.
‡Graduate Student Research Assistant, Department of Aerospace Engineering.
§A. B. M. Modine Professor, Department of Aerospace Engineering. Fellow AIAA.

established that soot surface oxidation in laminar diffusion flames, at fuel-rich and near-stoichiometric conditions, involving a variety of hydrocarbon fuels (acetylene, ethylene, propylene, propane, and benzene) was dominated by the reaction of the soot surface with OH and could be correlated effectively by estimating the oxidation rate due to O_2 using the classical expression of Nagle and Strickland-Constable[21] (whose results were later confirmed by Park and Appleton[22]) combined with an oxidation rate due to OH that had very nearly the same collision efficiency as the results of Neoh et al.,[23] Neoh,[24] and Neoh et al.[25] based on measurements in soot-containing premixed flames. This finding is also in fair agreement with earlier measurements of soot surface oxidation rates by OH in diffusion flames at atmospheric pressure due to Garo et al.[26,27] and Haudiquert et al.[28]

Naturally, there have been many other studies of the structure and soot reaction processes of laminar hydrocarbon-fueleddiffusion flames, seeking detailed models of their properties; see Balthasar et al.,[29] Bai et al.,[30] and references cited therein. Early measurements of the structure and soot reaction processes of laminar diffusion flames include the studies of Mitchell et al.,[31] Santoro et al.,[32] Smyth et al.,[33] Santoro et al.,[34] Puri et al.,[35,36] Saito et al.,[37] and many others reviewed by Haynes and Wagner,[11] Howard,[12] and Richter and Howard.[13] Additional work along these lines due to Garo et al.,[26,27] Haudiquert et al.,[28] and McEnally and Pfefferle,[38,39] McEnally et al.,[40] and Smooke et al.[41] involve sophisticated probe and nonintrusive measurements within soot-containing laminar diffusion flame environments. None of these studies, however, involve the full suite of measurements used by Xu et al.,[4,5] Xu and Faeth,[6,7] and Xu et al.[8] within laminar premixed and diffusion flames that is needed to evaluate theories of soot growth along the lines of Colket and Hall,[17] Frenklach and wang,[18,19] and Kazakov et al.[20]

Based on this status, the present investigation sought to improve understanding of the structure and soot surface growth properties of diffusion flames, by experimentally studying coflowing laminar jet diffusion flames burning in air at atmospheric pressure but considering hydrocarbons other than acetylene as the fuel to explore potential modifications of the soot surface growth mechanism when the fuel was no longer a species that is a direct reactant of the HACA soot surface growth mechanism, for example, ethylene, propylene, propane, and benzene considered as fuels, which is the case for acetylene that was considered earlier by Xu and Faeth.[7] In particular, benzene was considered to study the behavior of fuels more closely related to polycyclic aromatic hydrocarbons (PAH) than the other fuels that were studied because PAH soot surface growth mechanisms have been proposed as an alternative to HACA soot surface growth mechanisms; see Howard,[12] Richter and Howard,[13] and references cited therein. In addition, corrections of soot surface growth rates to account for effects of soot surface oxidation were improved compared to earlier work, for example, Refs. 4, 5, and 7, by exploiting the recent findings concerning soot surface oxidation rates in laminar diffusion flames at atmospheric pressure reported by Xu et al.[8]

To summarize, the specific objectives of the present study were as follows: 1) to measure the structure (temperatures, stable and radical species concentrations, and velocities) and soot properties (soot volume fractions and primary soot particle diameters) within the soot formation region of hydrocarbon-fueled laminar diffusion flames burning in air and 2) to exploit both the new measurements, along with results from existing measurements in premixed flames[4,5] and acetylene-fueled diffusion flames,[7] to evaluate and correlate the HACA soot surface growth mechanisms of Colket and Hall,[17] Frenklach and Wang,[18,19] and Kazakov et al.[20] The study was limited to measurements along the axes of buoyant laminar jet diffusion flames burning in coflowing air at atmospheric pressure, similar to earlier studies of soot processes in diffusion flames in this laboratory due to Sunderland et al.,[1] Sunderland and Faeth,[2] Xu and Faeth,[7] and Xu et al.[8]

Experimental Methods

Test Apparatus

Experimental methods were similar to those of Xu and Faeth[7] and Xu et al.[8] and will only be described briefly. The same burner was used to observe soot processes in laminar diffusion flames and to calibrate the H concentration measurements using a laminar premixed flame. The burner had a 34.8-mm-diam inner port both for the fuel stream of the diffusion flames and for the methane–oxygen–nitrogen reactant mixture of a premixed calibration flame that was used to calibrate present measurements of some radical species (H, OH, and O). A 60-mm-diam coannular outer port was used both for the dry air coflow of the diffusion flames and for the nitrogen coflow of a premixed calibration flame. The dry air coflow of the diffusion flames served to eliminate natural convection instabilities, to avoid problems of argon in natural air eluting with O_2 during gas chromatography measurements and contamination of the flames with the small levels of CO_2 and water vapor that are present in natural air. The nitrogen coflow of the premixed calibration flame served to eliminate the annular diffusion flame for this fuel-rich premixed flame to improve the accuracy of the H concentration calibration.

Burner gas flow rates were measured with rotameters. Mixtures were allowed to mix within feed lines that were at least 1000 diameters long to ensure that they were uniform. The flames burned in a room air environment with room disturbances controlled by surrounding them with several layers of screens and a plastic enclosure. The burner could be traversed horizontally and vertically to accommodate rigidly mounted optical instrumentation.

Instrumentation

Present measurements were similar to those in Refs. 7 and 8 and will only be described briefly. The following properties were measured along the axes of the test flames: soot volume fractions, flame temperatures, concentrations of major gas species, gas velocities, and concentrations of some radial species (H, OH, and O).

Soot volume fractions were measured by deconvoluting laser extinction measurements at 632.8 nm for chordlike paths through the flames. These data were reduced using the refractive indices of Dalzell and Sarofim[42] for consistency with past work[1–7]; however, these refractive index values have recently been confirmed by Krishnan et al.[43] The experimental uncertainties (95% confidence) of the soot volume fractions are estimated to be smaller than 10% for soot volume fractions greater than 0.02 ppm, increasing inversely proportional to the soot volume fraction for smaller values.

Soot and gas temperatures are essentially the same[7]; therefore, soot (gas) temperatures were measured by deconvoluting spectral radiation intensities for chordlike paths through the flames. Temperatures were computed based on spectral radiation intensities at several wavelength pairs, as follows: 550/700, 550/750, 550/830, 600/700, 600/750, 600/830, and 650/750 nm. Temperature differences between the average and any of the line pairs were less than 50–100 K, and experimental uncertainties (95% confidence) of the measurements were less than 50 K.

Concentrations of major stable gas species (N_2, H_2O, H_2, O_2, CO, CO_2, CH_4, C_2H_2, C_2H_4, C_2H_6, C_3H_6, C_3H_8, C_6H_6, and neon, the last being a tracer gas used to estimate effects of radial diffusion of lithium-containing species that were used to find H, OH, and O concentrations) were measured by sampling and gas chromatography. Experimental uncertainties (95% confidence) of these measurements are estimated to be less than 10% for stable gas species having concentrations greater than 0.1%, increasing to roughly 30% at the present limit of detection of stable gas species, brought to this level by repeated measurements to establish reliable calibrations and average concentration values for each species.

Soot primary particle diameters were measured using thermophoretic sampling and analysis by transmission electron microscopy (TEM) and high-resolution TEM (HRTEM). Thermophoretic soot sampling results are only reported here for the axes of the flames. Potential effects of contamination of these samples as the soot sampler traversed the flames when moving to-and-from the flame axes was established in two ways: 1) Sampling in the region before the onset of soot formation along the axes of the flames (but where there was a well-developed annular soot-containing region near the edge of the region exhibiting yellow soot luminosity)

Table 1 Summary of test laminar jet diffusion flames[a]

Parameter	Flame 1	2	3	4	5	6	7	8	9
Fuel	C_2H_2	C_2H_2	C_2H_2	C_2H_4	C_3H_6	C_3H_8	C_6H_6	C_6H_6	C_6H_6
Fuel in fuel stream, % by volume	16.9	15.1	17.3	100.0	18.8	100.0	0.6	1.3	2.2
C_2H_2 in fuel stream, % by volume[b]	——	——	——	——	——	——	14.0	10.2	5.5
N_2 in fuel stream, % by volume	83.1	84.9	82.7	——	81.2	——	85.4	88.5	92.3
Fuel stream flow, cm^3/s[c]	26.10	29.90	31.30	5.52	16.62	3.20	28.92	29.37	30.02
Dry air coflow, cm^3/s[c]	94.7	94.7	94.7	292.0	222.0	222.0	160.0	160.0	160.0
Luminous flame length, mm	82	80	103	100	100	100	90	90	90
Stoichiometric flame length, mm	100	106	116	81	74	79	95	130	110
Stoichiometric flame temperature, K[d]	2380	2320	2390	2370	2150	2260	2140	2050	1900

[a]Laminar round coflowing jet diffusion flames with a 34.8-mm inside diameter fuel port and a 60-mm inside diameter concentric dry air port, both directed vertically upward. Ambient temperature and pressure of 294 ± 2 K and 98 ± 1 kPa. Gas purities (% by volume) as follows: $N_2 = 99.9\%$, $O_2 = 99.6\%$, $C_2H_2 = 99.6\%$, $C_2H_4 = 99.5\%$, $C_3H_6 = 99.5\%$, $C_3H_8 = 99.5\%$; liquid C_6H_6 purity = 99.0%; dry air coflow consisted of 79% N_2 and 21% O_2.
[b]Unless acetylene is the fuel, in which case the concentration of acetylene in the fuel stream is indicated by % by volume fuel in the fuel stream.
[c]Volume flow rate based on standard conditions of 300 K and 101.3 kPa.
[d]Adiabatic flame temperature for stoichiometric combustion of the fuel stream in dry air with the reactants at 300 K and combustion at 101.3 kPa.

properly indicated that no soot aggregates, which could have been deposited as the sampler passed through the annular soot-containing region, were present on the sampler for the sampling conditions used during the present study. 2) The sampled soot exhibited only nearly constant primary soot particle diameters at each flame condition along the axis, for example, the standard deviations of primary particle diameters were less than 10%, rather than the widely varying primary soot particle diameters that would be observed if off-axis soot particles were present in the sample. The experimental uncertainties (95% confidence) of primary particle diameters at a point were estimated to be less than 10%.

Streamwise gas velocities were measured using laser velocimetry. The experimental uncertainties (95% confidence) of these measurements were less than 5%.

Measurements of H concentrations were carried out by deconvoluted absorption following the Li/LiOH absorption technique of Neoh et al.,[23] Neoh,[24] and Neoh et al.[25] Correction for the radial diffusion of lithium-containing compounds was found from measurements of the concentrations trace levels of neon in the fuel stream, when it was assumed that the diffusivities of the lithium-containing compounds and neon were similar. The H concentration measurements were calibrated using a premixed flame as discussed by Xu and Faeth,[7] similar to discussions in Refs. 23–25. Measurements using different seeding levels showed that effects of the lithium compounds used for the H concentration measurements were negligible, similar to past work.[6,7] Experimental uncertainties (95% confidence) of the H concentration measurements are estimated to be smaller than 30%. Given measured concentrations of H, O_2, H_2, and H_2O, values of OH and O concentrations were computed assuming partial equilibrium among these species following Refs. 23–25, using the equilibrium constant data of Chase et al.[44] This involved finding OH and O concentrations assuming partial equilibrium considering H, H_2O, and H_2 concentrations for fuel-rich conditions and H, H_2O, and O_2 concentrations for fuel-lean conditions. The experimental uncertainties of OH and O concentrations were comparable to those of H concentrations. The laminar premixed flame used to calibrate the H concentration measurements operated using the fuel port of the present burner; see Xu and Faeth[6] for a summary of the properties of this flame.

Test Conditions

The present results involve measurements from nine test flames: three acetylene–nitrogen-fueled flames drawn from the earlier work of Xu and Faeth,[7] an ethylene-fueled flame, a propylene–nitrogen-fueled flame, a propane-fueled flame, and three acetylene–benzene–nitrogen-fueled flames, with the last six flames measured during the present investigation. The test conditions for all nine flames are summarized in Table 1. Nitrogen dilution of the fuel stream was found to be a convenient way to reduce soot concentrations in the flames because rates of soot formation tend to be roughly proportional to the concentration of fuel at the burner exit, with little other effect on flame properties. Therefore, it was used for the acetylene-, propylene-, and acetylene–benzene-fueled flames to keep maximum soot volume fractions smaller than 2 ppm so that measurement problems due to large soot concentrations could be avoided. Luminous flame lengths were 80–103 mm, whereas stoichiometric flame lengths (the vertical heights where the local fuel-equivalence ratios at the axis were unity) were 74–130 mm. The stoichiometric flame temperatures in Table 1 were found from adiabatic combustion calculations using the algorithm of McBride et al.[45] Finally, acetone contamination of acetylene pointed out by Hamins et al.[46] and Colket et al.[47,48] are not thought to be a problem for present measurements, based on evaluation of this effect by Xu and Faeth[7] using flames 1–3 summarized in Table 1.

Results and Discussion

Soot Structure

Soot particles observed during the present investigation were similar to those seen during earlier studies of soot processes in laminar premixed and diffusion flames; see Refs. 1–8 and references cited therein. Figures 1a–1c show typical TEM (length scale of 100 nm) photographs and Figs. 1d–1f show HRTEM (length scale of 20 nm) photographs of soot particles along the axis of the ethylene/air flame (flame 4). Images of soot particles for the other flames studied were qualitatively the same. Images of soot particles are provided for conditions near the onset of soot formation, where primary soot particle diameters reach a maximum (Figs. 1a and 1d); near the end of soot formation, where soot concentrations reach a maximum (Figs. 1b and 1e); and near stoichiometric conditions, where soot oxidation is roughly 90% complete (on a mass basis) for this flame (Figs. 1c and 1f). The TEM images indicate that soot particles consist of roughly spherical primary soot particles with the mean number of primary soot particles per aggregate progressively increasing with increasing elapsed time (or streamwise distance) in the flame. A nonintuitive feature of the results shown in Fig. 1 is that after an initial rapid increase of primary soot particle diameters, just after the onset of soot formation along the axis of the flames, mean primary soot particle diameters subsequently decrease with increasing distance from the burner exit in spite of effects of soot surface growth throughout the remainder of the soot formation region. This behavior has been observed for all of the laminar jet diffusion flames studied in this laboratory[1–3,7] and will be discussed more fully when flame structure is discussed.

The HRTEM images in Figs. 1d–1f also are similar to soot aggregates observed during past studies of soot formation in flames; see Lahay and Prado,[49] Garo et al.,[50] Hess and Herd,[51] Ishiguro et al.[52] and references cited therein for other examples. In general,

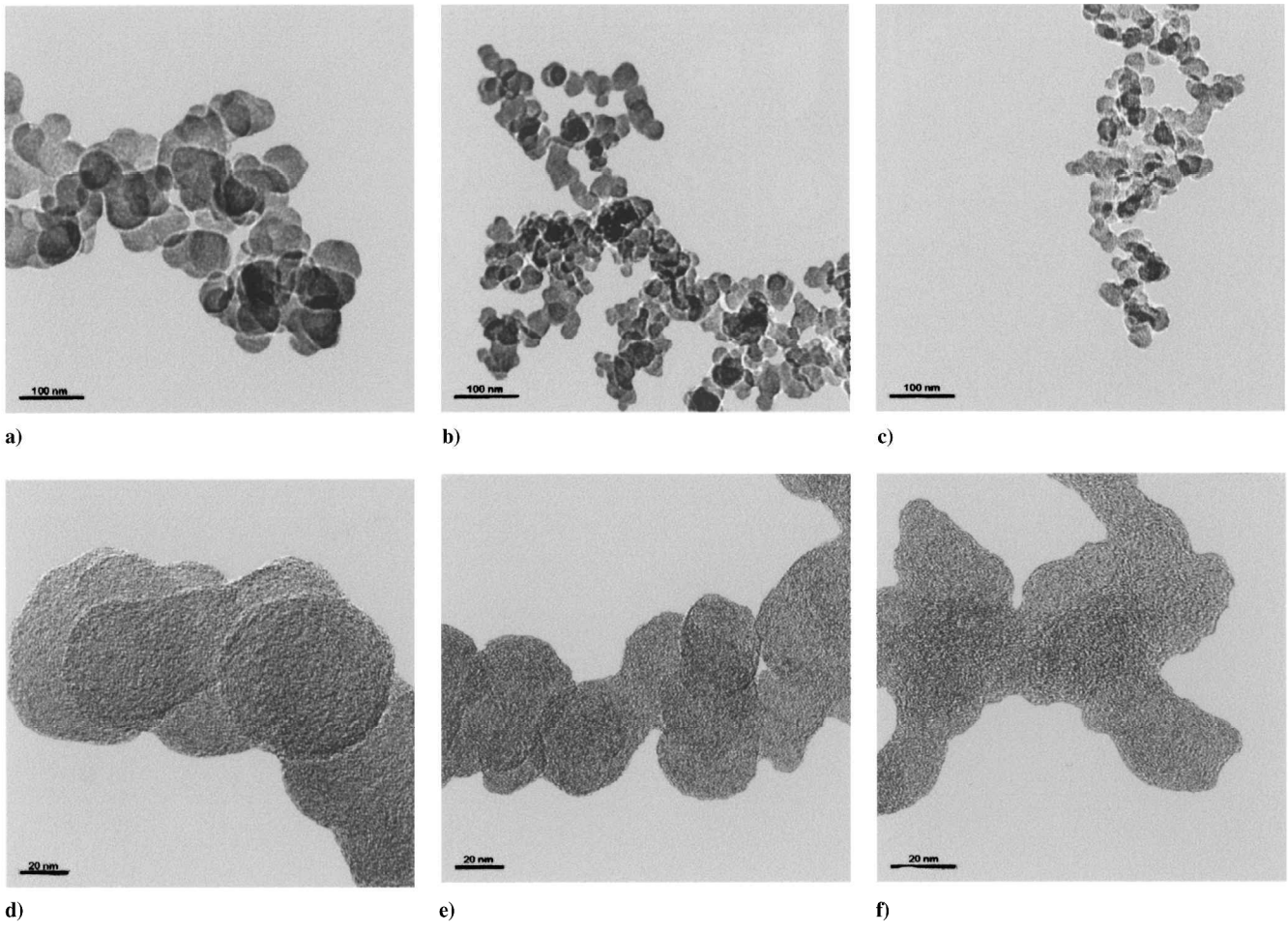

Fig. 1 Photographs of soot aggregates along the axis of the ethylene/air laminar jet diffusion flame at atmospheric pressure (flame 4): a) TEM, maximum primary particle diameter location ($z \sim 35$ mm), b) TEM, maximum soot volume fraction location ($z \sim 55$ mm), c) TEM, nearly at end of soot-containing region, where soot oxidation is roughly 90% complete ($z \sim 80$ mm), d) HRTEM, maximum primary particle diameter location ($z \sim 35$ mm), e) HRTEM, maximum soot volume fraction location ($z \sim 55$ mm), and f) HRTEM, nearly at end of soot-containing region, where soot oxidation is roughly 90% complete ($z \sim 8$ mm).

the primary soot particles near the maximum primary soot particle size position (Fig. 1d) and the maximum soot concentration position (Fig. 1e) exhibit an outer shell having a sheetlike structure parallel to the surface of the primary soot particle and an inner core that appears to result from coalescence of several smaller primary soot particles near the soot nucleation condition. The irregular structure of the inner core is more evident after the shell-like surface layer has been largely oxidized away (Fig. 1f). Other evidence of the different character of the center and surface layers of primary soot particles is provided by the different densities and oxidation properties of the centers of primary soot particles compared to their near-surface conditions.[25]

Flame Structure

Measurements of gas (soot) temperatures, streamwise gas velocities, soot volume fractions, primary soot particle diameters, concentrations of major gas species, and concentrations of radical species (H, OH, and O) are plotted as a function of height above the burner exit for an acetylene–nitrogen/air flame (flame 2), the ethylene/air flame (flame 4), and an acetylene–benzene–nitrogen/air flame (flame 9) in Figs. 2–4. Note that the structure of the acetylene–nitrogen/air flame (flame 2) shown in Fig. 2 is typical of the other acetylene–nitrogen/air flames (flames 1 and 3), that the structure of the ethylene/air flame (flame 4) shown in Fig. 3 is typical of the propylene–nitrogen/air and propane/air flames (flames 5 and 6), and that the structure of the acetylene–benzene–nitrogen/air flame (flame 9) shown in Fig. 4 is typical of the other acetylene–benzene–nitrogen/air flames (flames 7 and 8). Elapsed times in the flames, found by integrating the streamwise velocity measurements along the axes of the flames, are indicated at the tops of Figs. 2–4. These elapsed times are relative to the first streamwise measuring station where detectable soot volume fractions were observed ($z = 10$ mm). The stoichiometric ($\phi = 1$), or flame sheet condition, is marked for the ethylene/air flame (flame 4) shown in Fig. 3 (at $z = 82$ mm); however, the flame sheet lies beyond the region illustrated for the acetylene–nitrogen/air flame (flame 2) shown in Fig. 2 (at $z = 106$ mm) and for the acetylene–benzene–nitrogen/air flame (flame 9) shown in Fig. 4 (at $z = 110$ mm). Thus, all properties shown for the acetylene–nitrogen/air and acetylene–benzene–nitrogen/air flames are for fuel-rich conditions. The ends of the luminous flame regions in Figs. 2–4 are at $z = 80$, 100, and 90 mm although soot concentrations near these boundaries were too small to be accurately measured and reported using the present laser extinction technique. Finally, it is convenient to divide the present flames into two regions separated by the location of the maximum soot concentration condition as follows: 1) the region upstream of this condition where soot formation dominates other soot reaction processes and soot concentrations increase with increasing distance from the burner exit, which will be called the soot formation region, and 2) the region downstream of this condition where soot oxidation dominates other soot reaction processes and soot concentrations decrease with increasing distance from the burner exit, which will be called the soot oxidation region.

Gas (soot) temperatures in Figs. 2–4 reach a broad maximum in the soot formation region somewhat before the flame sheet is reached. The temperature range in the soot formation regions of the present flames is relatively narrow, roughly 1600–1850 K. Kent and Wagner[53,54] and Boedeker and Dobbs[55,56] have pointed out that

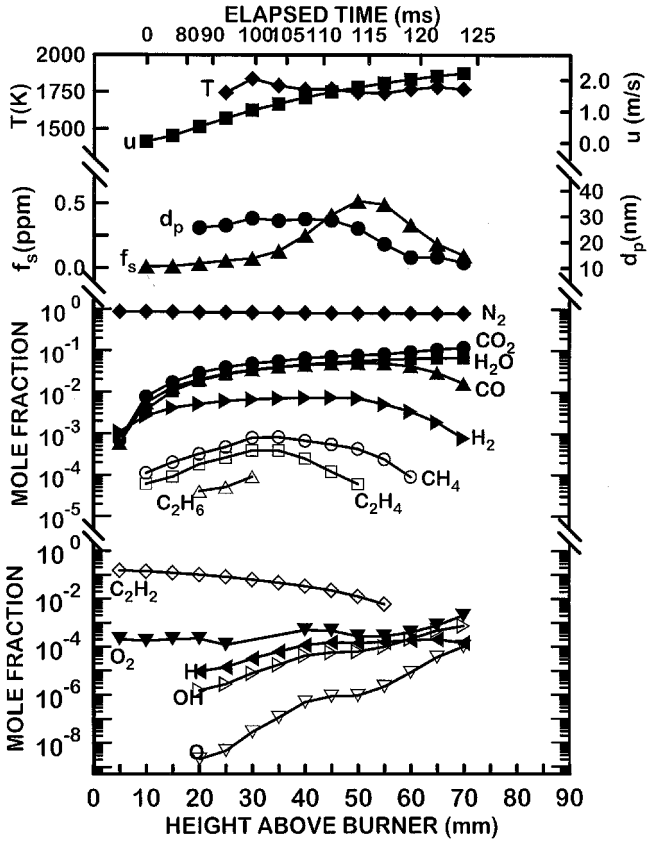

Fig. 2 Measured soot and flame properties of an acetylene-fueled laminar jet diffusion flame burning in coflowing air at atmospheric pressure; flame 2, fuel stream of 15.1% C_2H_2 and 84.9% N_2 by volume (from Xu and Faeth[7]).

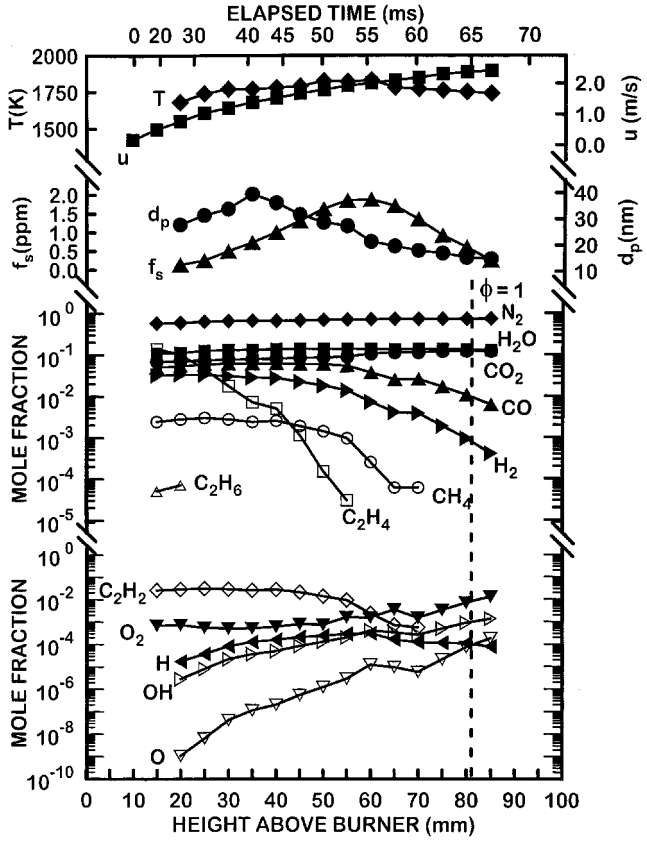

Fig. 3 Measured soot and flame properties of an ethylene-fueled laminar jet diffusion flame burning in coflowing air at atmospheric pressure; flame 4, fuel stream of 100% C_2H_4 by volume.

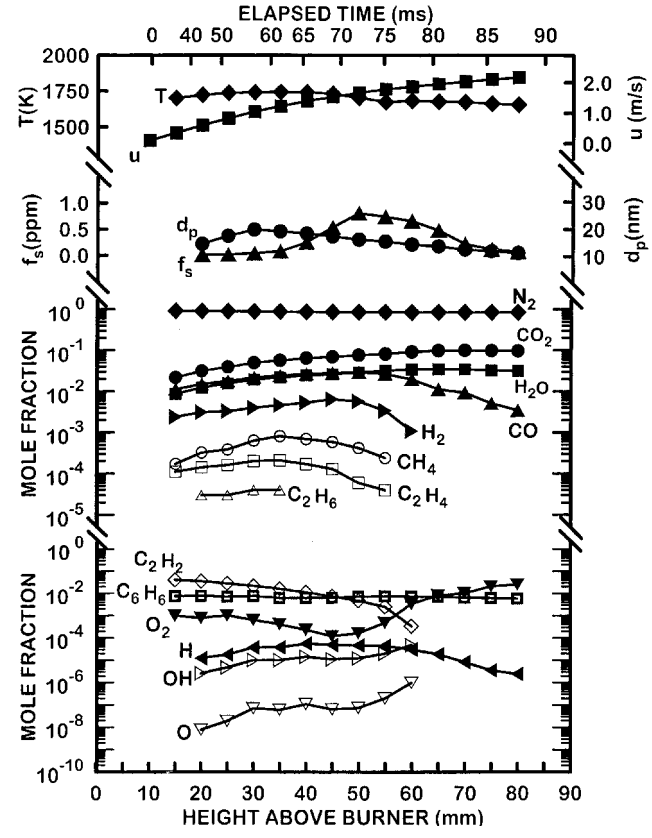

Fig. 4 Measured soot and flame properties of an acetylene–benzene-fueled laminar jet diffusion flame burning in coflowing air at atmospheric pressure; flame 9, fuel stream of 2.2% C_6H_6, 5.5% C_2H_2, and 92.3% N_2 by volume.

maximum temperatures in soot-containing diffusion flames are significantly reduced from adiabatic flame temperatures due to continuum radiation heat losses from soot. The present flames, as well as earlier diffusion flames studied in this laboratory,[1–3,7] exhibit maximum temperatures smaller than adiabatic flame temperatures (Table 1) for similar reasons.

Gas velocities in Figs. 2–4 increase with increasing distance from the burner exit due to effects of buoyancy, for example, burner exit velocities are 0.003–0.03 m/s, whereas maximum measured velocities are in excess of 2 m/s. This causes corresponding distortion of the elapsed timescale at the tops of Figs. 2–4.

Primary soot particle diameters reach maximum values relatively early in the soot formation region in Figs. 2–4, as already noted in connection with Fig. 1. This behavior is caused by accelerating soot primary particle nucleation rates with increasing streamwise distance, which is caused by progressively increasing H concentrations with increasing streamwise distance as discussed by Xu and Faeth.[7] This behavior causes the relatively few primary soot particles formed near soot inception conditions that become large due to long periods of soot surface growth in a region where acetylene concentrations are large, to be superseded by the much larger number of primary soot particles formed later in the soot-formation region that are smaller due to shorter periods of soot surface growth in regions where growth rates are reduced due to smaller acetylene concentrations. This trend is aided because soot growth remains relatively rapid near soot inception conditions, as noted by Tesner,[57,58] which allows the few primary particles present at this location to grow relatively large.

Significant levels of soot formation (evidenced by the appearance of finite levels of soot volume fractions) are generally associated with conditions where detectable levels of H were first observed, for example, where H concentrations exceed 10 ppm in Figs. 2–4. For all of the fuels, this condition also involved relatively large acetylene concentrations, for example, values of 4–10% by volume for the conditions shown in Figs. 2–4. Soot formation again

became small when maximum soot concentrations were reached, which occurred in the presence of relatively large concentrations of H (100–200 ppm), where acetylene concentrations became smaller than roughly 1% by volume. An interesting feature of the maximum soot concentration condition where soot formation becomes small when benzene is a portion of the fuel, for example, in Fig. 4, is that this event is definitely correlated with conditions where acetylene becomes small, whereas the concentrations of benzene remain relatively constant in this region. (See the region near the maximum soot concentration conditions in Fig. 4.)

The concentrations of major stable gas species in Figs. 2–4 are similar to observations in other laminar diffusion flames that have been studied, for example, Refs. 1–3. When acetylene is the fuel, for example, in Fig. 2, its concentration progressively decreases with increasing distance from the burner exit. For fuels other than acetylene, for example, Figs. 3 and 4, however, the original fuel generally disappears relatively soon within the soot formation region to yield hydrogen and hydrocarbon species that are relatively robust in high-temperature flame environments, particularly relatively stable acetylene. Acetylene is especially important as a fuel decomposition product because it is thought to be the major building block of both PAH, which leads to soot nucleation, and soot surface growth.[12,17–20] Benzene as a fuel is an apparent exception to this behavior (Fig. 4), but even benzene largely disappears near the burner exit, leaving a relatively small but nearly constant benzene concentration in the soot-containing region with benzene only finally disappearing near the flame sheet. In fact, concentration distributions of acetylene within flames fueled with hydrocarbons other than acetylene are qualitatively similar to concentration distributions of acetylene within flames fueled with acetylene. The final combustion products, CO_2 and H_2O, increase with increasing streamwise distance throughout the soot formation region, reaching broad maxima near the flame sheet ($\phi = 1$). Intermediate combustion products associated with water–gas equilibrium, CO and H_2, are present in relatively large concentrations throughout the soot formation region, reaching broad maxima somewhat upstream of the flame sheet. Finally, nitrogen concentrations remain relatively uniform for the flame regions shown in Figs. 2–4.

Concentrations of O_2 either progressively increase with increasing distance from the burner exit (Figs. 2 and 3) or progressively increase as the flame sheet is approached after reaching a broad minimum near the burner exit (Fig. 4). The former behavior follows because O_2 concentrations at the flame sheet are relatively large. The latter behavior is probably caused by some leakage of coflowing O_2 into the fuel-rich region of the flames through the gap between the burner exit and the point where the flames are attached, similar to behavior observed by Mitchell et al.[31] for a methane/air laminar coflowing jet diffusion flame. Thus, O_2 is invariably present at concentrations on the order of 0.1% (by volume) throughout most of the soot formation region of the present flames. In addition, concentrations of fuellike species, particularly H_2 and CO, penetrate well into the fuel-lean region. Thus, the present flames generally do not satisfy approximations made during simplified classical analysis of laminar diffusion flames in that there is considerable overlap of fuel- and oxidantlike species in the region of the flame sheet.

Concentrations of OH and O increase monotonically as the flame sheet is approached, whereas concentrations of H reach a broad maximum within the soot formation region before decreasing somewhat as the flame sheet is approached. Similar to recent numerical predictions of the structure of soot-containing laminar coflowing jet diffusion flames at atmospheric pressure involving methane/air and ethylene/air as reactants due to McEnally et al.[40] and Smooke et al.,[41] near-equilibrium radical concentrations (based on present measurements of stable species concentrations and temperatures and the thermochemical data of Chase et al.[44]) were observed near the onset of soot formation, but OH concentrations eventually reach values 10–20 times larger than equilibrium concentrations near the flame sheet. In addition, concentrations of H exhibit superequilibrium properties at fuel-rich conditions similar to the superequilibrium properties of OH. Concentrations of O, however, become 100–1000 times larger than equilibrium concentrations as the flame sheet is approached; nevertheless, concentrations of O generally are 100–1000 times smaller than H and OH concentrations throughout most of the soot formation region. Finally, species that past measurements in diffusion flames have shown to be responsible for soot surface growth (C_2H_2 and H) (Ref. 7) and for soot surface oxidation (O_2 and OH) (Ref. 8) are seen to all be present within the soot formation region. Therefore, soot surface growth and oxidation proceed at the same time in the soot formation regions of the present diffusion flames. Notably, this behavior is also typical of past observations of soot surface growth in diffusion flames in this laboratory.[1–3,7]

Soot Surface Growth Rates

Past and present measurements were used to find soot surface growth rates for laminar premixed and diffusion flames. Major assumptions were identical to earlier work[1–7] as follows: 1) Soot mass production is dominated by soot surface growth rather than primary soot particle nucleation. 2) Effects of diffusion (Brownian motion) and thermophoresis on soot motion are small so that soot particles convect along the axes of the flames at the local gas velocity. 3) The density of soot is constant (taken to be 1850 kg/m^3 from Ref. 1). 4) The surface area available for soot growth is equivalent to constant diameter spherical primary soot particles that meet at a point. The justification of these assumptions and the detailed methods of finding soot surface growth rates from the present measurements are described in Refs. 1 and 7 and will not be repeated here. The experimental uncertainties (95% confidence) of soot surface growth rates are estimated to be less than 30%.

To interpret the present soot surface growth rates, gross soot surface growth rates were corrected for effects of soot surface oxidation because soot surface growth and oxidation proceed at the same time as just noted. A recent study of soot surface oxidation in laminar jet diffusion flames burning in coflowing air at atmospheric pressure,[8] which included all of the flames considered during the present investigation, indicated that soot surface oxidation in these flames proceeded via the OH soot surface oxidation mechanism described in Refs. 23 and 24 with nearly the same collision efficiency, after allowing for the relatively small contribution of direct soot oxidation based on the O_2 soot surface oxidation mechanism of Nagle and Strickland-Constable.[21] For example, the OH collision efficiency described in Refs. 23 and 24 is 0.13 with an uncertainty (95% confidence) of ± 0.03 based on measurements within premixed flames, whereas the OH collision efficiency of Xu et al.[8] is 0.14 and with an uncertainty (95% confidence) of ± 0.04 based on measurements within diffusion flames. Thus, all of the measurements of soot surface growth considered in the following, including earlier measurements in laminar premixed[4,5] and diffusion flames,[7] were corrected for effects of soot surface oxidation using the OH and O_2 approach based on the measurements of Xu et al.[8] It was found that effects of soot surface oxidation estimated in this way generally were small, except when soot surface growth rates became small toward the end of the soot formation region. To be conservative about potential effects of soot surface oxidation, however, determinations of soot surface growth rates corrected for effects of soot surface oxidation were limited to conditions where estimated soot surface oxidation rates never exceeded half the gross soot surface growth rates, similar to past work.[1–5,7]

To baseline the present estimates of soot surface growth rates with earlier studies of soot surface growth rates in laminar premixed and diffusion flames,[1–5,7] soot surface growth rates were also corrected for effects of soot surface oxidation using the same method as these earlier studies. During these earlier studies, rates of soot surface oxidation were estimated using approximate earlier methods based on the assumption that soot oxidation occurred by reaction with stable oxygen-containing species because concentrations of radical species were unknown. The simplified soot oxidation mechanism used for these estimates was as follows[1–5,7]: soot surface oxidation by O and OH was ignored, soot surface oxidation by O_2 was based on the results of Nagle and Strickland-Constable,[21] and soot surface oxidation by H_2O and CO_2 was estimated following Libby and Blake[59,60] and Johnstone et al.,[61] which yielded results similar to Bradley et al.[62] Similar to the present approach considering soot surface oxidation by OH and O_2, these estimates of net soot surface

growth rates were limited to conditions where estimated soot surface oxidation rates never exceeded half the gross soot surface growth rates, which also was similar to past work in this laboratory.[1–5,7] As a result of this conservative approach, soot surface growth rates corrected for soot oxidation found using the present O_2 and OH approach were essentially the same as those found using the earlier O_2, H_2O, and CO_2 approach.

Soot surface growth rates were interpreted using the HACA mechanisms described in Refs. 17–20 to maintain consistency with past evaluations of these mechanisms based on measurements of soot surface growth rates in premixed ethylene/air and methane/oxygen flames[4,5] and in acetylene–nitrogen/air diffusion flames.[7] In all cases, net soot surface growth rates corrected for soot surface oxidation were expressed as follows:

$$w_g = \alpha_i R_i \tag{1}$$

where i = CH or FW found from the measurements. The details of these mechanisms, the formulas for the R_i, and the reaction rate parameters used when computing values of the R_i can be found in the work by Xu et al.[4] The parameters α_i are empirical steric factors on the order of unity, with α_{CH} specified to be a constant[17] and α_{FW} specified to be a function of temperature.[18–20]

As a first approximation for all of the premixed and diffusion flames considered during this study, the R_i are proportional to the product $[H][C_2H_2]$. Thus, values of $w_g/[C_2H_2]$ measured for the premixed ethylene/air flames by Xu et al.,[4] the premixed methane/oxygen flames by Xu et al.,[5] the acetylene–nitrogen/air diffusion flames by Xu and Faeth,[7] and the present diffusion flames (after correcting all measurements for soot surface oxidation using the OH and O_2 approach based on the measurements of Xu et al.[8]), are plotted as a function of [H] in Fig. 5, to provide a direct test of the main features of the HACA soot surface growth mechanism without the intrusion of uncertainties due to the numerous empirical parameters in the original detailed mechanisms. The results for premixed and diffusion flames in Fig. 5 are distinguished by denoting them by open and solid symbols, respectively. An empirical correlation of the measurements is also given in Fig. 5, obtained as an average for all of the flames. There is a tendency for $w_g/[C_2H_2]$ to be slightly larger for diffusion flames than for premixed flames, at a given value of [H], when plotted in this manner. This is largely due to the approximation of the entire HACA mechanisms by the leading-term product, $[C_2H_2][H]$, because differences between overall environments of the soot formation regions of premixed and diffusion flames affect the higher-order reaction terms of the HACA mechanisms, for example, the near-equilibrium and superequilibrium radical concentrations of premixed and diffusion flames, respectively. It will be seen subsequently that no distinction between premixed and diffusion flames is observed when the full HACA mechanisms are considered. Nevertheless, the correlation of the results according to the crude $[C_2H_2][H]$ approximation of the more complete HACA mechanisms is surprisingly good, and soot surface growth rate properties in premixed and diffusion flames are reasonably consistent with each other in spite of the fundamental differences between the soot formation environments that can be seen by comparing the measured structures of the premixed flames,[4–6] with those of the diffusion flames seen in Ref. 7 and Figs. 2–4. Finally, the strong effect of [H] on w_g, evident from the results shown in Fig. 5, combined with the near-equilibrium and strongly superequilibrium behavior of H concentrations in premixed and diffusion flames, respectively, are responsible for the rather poor correlations and enhanced apparent soot surface growth rates of diffusion flames compared to premixed flames, when attempts are made to correlate soot surface growth rates in terms of acetylene concentrations and temperatures alone.[1]

A more direct evaluation of the HACA mechanisms of soot surface growth rates is obtained by plotting w_g directly as a function of R_{CH} for the Ref. 17 mechanism and as a function of $\alpha_{FW} R_{FW}$ (after correlating α_{FW} as a function of temperature) for the Ref. 18–20 mechanism. Results of this type for the Colket and Hall[17] mechanism are shown in Fig. 6. In Fig. 6, available measurements for both premixed and diffusion flames (after correcting all measurements for soot surface oxidation using the OH and O_2 approach based on the measurements of Xu et al.[8]) are illustrated, along with the best-fit correlation for all of the flames. The corresponding steric factor and its experimental uncertainties (95% confidence) is 1.0 with an uncertainty of ±0.2. First, it is encouraging that the steric factor is an order of magnitude unity, as expected.[17] Next, it is evident that use of the Colket and Hall[17] mechanism improves the correlation of soot surface growth rates in Fig. 6, compared to the approximate correlation based on only the leading terms of the HACA mechanism shown in Fig. 5. In addition, the correlation of the soot surface growth rate results for premixed and diffusion flames using the Colket and Hall[17] mechanism is essentially the same, that is, there is no statistical significance for the differences between the steric factors found for the data from the premixed and diffusion flames. Finally, considering results for the diffusion flames alone, there clearly is no difference between estimates of w_g based on the

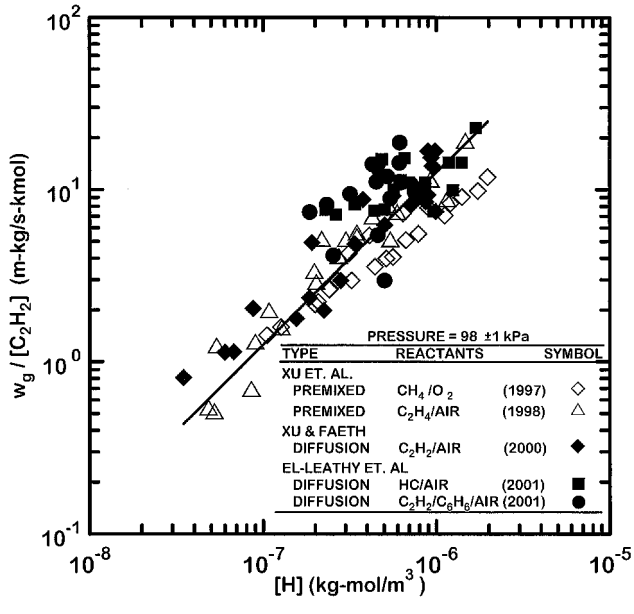

Fig. 5 Soot surface growth rates (corrected for soot surface oxidation) as a function of acetylene and H concentrations for laminar flames at atmospheric pressure.

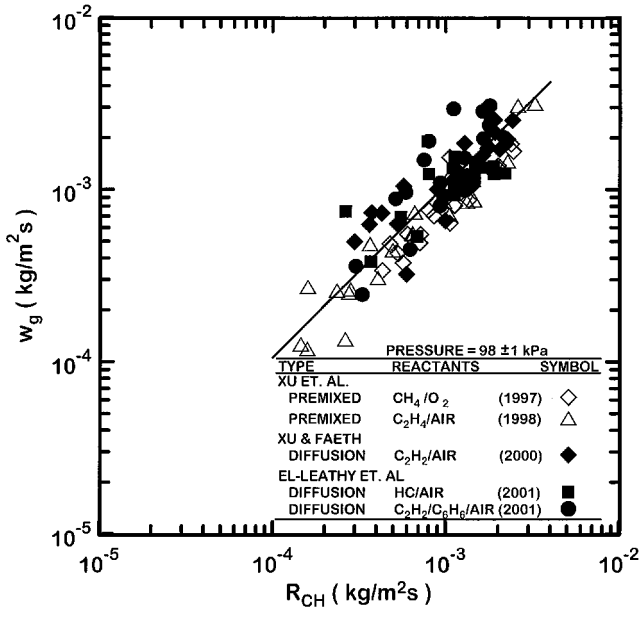

Fig. 6 Soot surface growth rates (corrected for soot surface oxidation) in terms of the HACA mechanism of Colket and Hall[17] for laminar flames at atmospheric pressure.

HACA mechanism of Colket and Hall[17] as the hydrocarbon fuel type is varied among the alkyne, alkene, alkane, and aromatic fuels considered during the present investigation, that is, there is no statistical significance to the differences between the values of the steric factors found for the various hydrocarbon fuels in diffusion flames that were considered during the present and past studies illustrated in Fig. 6.

The correlation of α_{FW} for soot surface growth for the complete database of laminar premixed and diffusion flames (corrected for soot surface oxidation similar to the results shown in Figs. 5 and 6) was essentially the same as the results presented in the diffusion flame study of Xu and Faeth,[7] which considered all of the premixed flames but was limited to the acetylene/air diffusion flames. A complete plot of these results can be found in El-Leathy.[9] The correlation of all of the soot surface growth rate data considered here, assuming that $\alpha_{FW}(T)$ could be represented by an Arhennius function similar to that in Ref. 7, yielded

$$\alpha_{FW}(T) = 0.0017 \exp(12{,}100/T) \qquad (2)$$

The subsequent plot of w_g as a function of $\alpha_{FW} R_{FW}$ was qualitatively similar to the plot (Fig. 8) shown in Ref. 7. These results indicated that correlations of measurements in laminar premixed and diffusion flames were essentially the same, that effects of fuel type for laminar premixed and diffusion flames were small, that values of α_{FW} were on the order of unity as expected, and that the negative activation energy implied by the argument of the exponential factor of Eq. (2) corresponds to behavior anticipated in Refs. 18–20 for soot surface growth mechanism.

Similar to earlier findings for soot surface growth rates,[4,5,7] the HACA soot surface growth rate mechanisms described in Refs. 17–20 continue to be encouraging, and they may eventually provide the basis for reliable methods to estimate soot surface growth rates in flame environments fueled with hydrocarbons. Uncertainties remain, however, about effects of pressure, effects of temperature outside the limited range considered here, and effects of PAH as fuels on soot surface growth rates in premixed and diffusion flames.

Conclusions

Flame structure and soot surface growth rates were studied for coflowing, laminar jet diffusion flames. Test conditions involved acetylene-, ethylene-, propylene-, propane-, and benzene-fueled diffusion flames burning in coflowing dry air at atmospheric pressure with the reactants at normal temperature and pressure as summarized in Table 1 (after supplementing present measurements with those of Xu and Faeth[7] for acetylene-fueled diffusion flames). Information about soot surface growth rates in these diffusion flames was also supplemented by earlier measurements in laminar premixed ethylene/air and methane/oxygen flames due to Xu et al.,[4,5] which were also observed at atmospheric pressure with the reactants at normal temperature. The major conclusions of the study are as follows:

1) In all flames that have been considered thus far (except naturally for acetylene-fueled flames), the original fuel largely decomposes relatively early in the soot formation process, yielding species that generally are associated with soot surface growth and oxidation, for example, C_2H_2, H, and OH, among others. The yields of these species are affected by the flame type (premixed or diffusion flame), the fuel and oxidizing species, and the flame operating conditions; however, subsequent reaction of these materials during processes of soot surface growth is largely dependent on local flame conditions and is not materially affected by the fuel or oxidant type or whether these processes are occurring in premixed or diffusion flame environments.

2) Soot surface growth rates in laminar premixed and diffusion flames, for various fuel and oxidant types, agree within experimental uncertainties at comparable local conditions and could be correlated reasonably well using the HACA soot surface growth mechanisms described in Refs. 17–20 with the steric factors of both these mechanisms having values on the order of unity, as anticipated.

3) Measurements in all the diffusion flames indicate that H, OH, and O approach equilibrium near the start of the soot formation region, but generally exhibit superequilibrium concentrations throughout the soot-containing region (with H and OH reaching superequilibrium ratios of 10–20 and O reaching superequilibrium ratios of 100–1000, although actual concentrations of O generally are much smaller than the concentrations of H and OH).

4) Measurements in the diffusion flames showed that significant degrees of soot formation begins near the jet exit once H first appears in a prevailing condition where acetylene concentrations are relatively large and that soot formation ends near the flame sheet where acetylene disappears in a prevailing condition where H concentrations are relatively large. This behavior is consistent with soot surface growth being dominated by the HACA mechanisms as noted in connection with conclusion 2. Finally, benzene was only observed for the benzene-fueled flames where benzene concentrations were both constant and relatively small (less than 1% by volume) throughout the soot-containing region and were not particularly correlated with either the onset or the end of soot formation.

5) The present investigation exploited recent measurements of soot surface oxidation rates in laminar diffusion flames (including all of the flames considered here) due to Xu et al.[8] to correct gross measurements of soot surface growth rates for simultaneous effects of soot surface oxidation. This involved estimating soot surface oxidation rates by O_2 based on the results of Ref. 21 and by OH as proposed in Refs. 23–25, but using nearly the same OH collision efficiency of Ref. 8. Corrected soot surface growth rates were only considered, however, in cases where estimated soot surface oxidation rates were less than half the gross soot surface growth rates for all flame conditions considered here, which is the same approach used during earlier studies where other mechanisms of soot surface oxidation were considered.[4,5,7] Because of this relatively conservative approach for correcting soot surface growth rates for effects of soot surface oxidation, however, present estimates of net soot surface growth rates were essentially unchanged from earlier results where soot surface oxidation was estimated using an approximate method based on the concentrations of stable species (O_2, H_2O, and CO_2) because radical concentrations needed for the OH/O_2 soot surface oxidation mechanism were not known.[4,5,7]

Note that measurements used for soot surface growth rate results reported here, for example, Refs. 4, 5, and 7 and the present investigation, are limited to hydrocarbon-fueled flames at atmospheric pressure with the reactants initially at normal temperature. These conditions yielded ranges of properties for conditions where the soot surface growth rates were measured as follows: H atom concentrations of 3×10^{-8}–2×10^{-6} kgmol/m^3, C_2H_2 concentrations of 6×10^{-6}–2×10^{-3} kgmol/m^3, temperatures of 1600–1850 K, and original fuels involving alkynes, alkenes, alkanes, and aromatics (C_2H_2, C_2H_4, C_3H_6, C_3H_8, and C_6H_6). Use of the present correlations of soot surface growth rates for other flame conditions should be approached with caution.

Acknowledgments

This research was supported by NASA Grants NAG3-1245, 1878, and 2048 under the technical management of D.L. Urban and Z.-G. Yuan of NASA John H. Glenn Research Center at Lewis Field.

References

[1] Sunderland, P. B., Köylü, Ü. Ö., and Faeth, G. M., "Soot Formation in Weakly Buoyant Acetylene-Fueled Laminar Jet Diffusion Flames Burning in Air," *Combustion and Flame*, Vol. 100, Nos. 1/2, 1995, pp. 310–322.

[2] Sunderland, P. B., and Faeth, G. M., "Soot Formation in Hydrocarbon/Air Laminar Jet Diffusion Flames," *Combustion and Flame*, Vol. 105, Nos. 1/2, 1996, pp. 132–146.

[3] Lin, K.-C., Sunderland, P. B., and Faeth, G. M., "Soot Nucleation and Growth in Acetylene/Air Laminar Coflowing Jet Diffusion Flames," *Combustion and Flame*, Vol. 104, No. 3, 1996, pp. 369–375.

[4] Xu, F., Sunderland, P. B., and Faeth, G. M., "Soot Formation in Laminar Premixed Ethylene/Air Flames at Atmospheric Pressure," *Combustion and Flame*, Vol. 108, No. 4, 1997, pp. 471–493.

[5] Xu, F., Lin, K.-C., and Faeth, G. M., "Soot Formation in Laminar Premixed Methane/Oxygen Flames at Atmospheric Pressure," *Combustion and Flame*, Vol. 115, Nos. 1/2, 1998, pp. 195–209.

[6] Xu, F., and Faeth, G. M., "Structure of the Soot Growth Region of Laminar Premixed Methane/Oxygen Flames," *Combustion and Flame*, Vol. 121, No. 4, 2000, pp. 640–650.

[7]Xu, F., and Faeth, G. M., "Soot Formation in Laminar Acetylene/Air Diffusion Flames at Atmospheric Pressure," *Combustion and Flame*, Vol. 125, Nos. 1/2, 2001, pp. 804–819.

[8]Xu, F., El-Leathy, A. M., Kim, C.-H., and Faeth, G. M., "Soot Surface Oxidation in Laminar Hydrocarbon/Air Diffusion Flames at Atmospheric Pressure," *Combustion and Flame* (to be published).

[9]Xu, F., "Soot Growth in Laminar Premixed Flames," Ph.D. Dissertation, Dept. of Aerospace Engineering, Univ. of Michigan, Ann Arbor, MI, June 1999.

[10]El-Leathy, A. M., "Effect of Hydrocarbon Fuel on Soot Surface Growth and Oxidation in Laminar Diffusion Flames," Ph.D. Dissertation, Mechanical Power Dept., Helwan Univ., Cairo, June 2002.

[11]Haynes, B. S., and Wagner, H. G., "Soot Formation," *Progress in Energy and Combustion Science*, Vol. 7, No. 4, 1981, pp. 229–273.

[12]Howard, J. B., "Carbon Addition and Oxidation Reactions in Heterogeneous Combustion and Soot Formation," *Proceedings of the Combustion Institute*, Vol. 23, 1990, pp. 1107–1127.

[13]Richter, H., and Howard, J. B., "Formation of Polycyclic Aromatic Hydrocarbons and Their Growth to Soot—A Review of Chemical Reaction Pathways," *Progress in Energy and Combustion Science*, Vol. 26, Nos. 4–6, 2000, pp. 565–608.

[14]Kennedy, I. M., "Models of Soot Formation and Oxidation," *Progress in Energy and Combustion Science*, Vol. 23, No. 2, 1997, pp. 95–132.

[15]Harris, S. J., and Weiner, A. M., "Surface Growth of Soot Particles in Premixed Ethylene/Air Flames," *Combustion Science and Technology*, Vol. 31, 1983, Nos. 3 and 4, pp. 155–167.

[16]Ramer, E. R., Merklin, J. F., Sorensen, C. M., and Taylor, T. W., "Chemical and Optical Probing of Premixed Methane/Oxygen Flames," *Combustion Science and Technology*, Vol. 48, Nos. 5 and 6, 1986, pp. 241–255.

[17]Colket, M. B., and Hall, R. J., "Successes and Uncertainties in Modelling Soot Formation in Laminar Premixed Flames," *Soot Formation in Combustion*, edited by H. Bockhorn, Springer-Verlag, Berlin, 1994, pp. 442–470.

[18]Frenklach, M., and Wang, H., "Detailed Modeling of Soot Particle Nucleation and Growth," *Proceedings of the Combustion Institute*, Vol. 23, 1999, pp. 1559–1556.

[19]Frenklach, M., and Wang, H., "Detailed Modeling of Soot Particle Nucleation and Growth," *Soot Formation in Combustion*, edited by H. Bockhorn, Springer-Verlag, Berlin, 1994, pp. 165–192.

[20]Kazakov, A., Wang, H., and Frenklach, M., "Detailed Modeling of Soot Formation in Laminar Premixed Ethylene Flames at a Pressure of 10 Bar," *Combustion and Flame*, Vol. 110, Nos. 1/2, 1995, pp. 111–120.

[21]Nagle, J., and Strickland-Constable, R. F., "Oxidation of Carbon Between 1000–2000°C," *Proceedings of Fifth Carbon Conference*, Vol. 1, 1962, pp. 154–164.

[22]Park, C., and Appleton, J. P., "Shock-Tube Measurements of Soot Oxidation Rates," *Combustion and Flame*, Vol. 20, No. 3, 1973, pp. 369–379.

[23]Neoh, K. G., Howard, J. B., and Sarofim, A. F., "Soot Oxidation in Flames," *Particulate Carbon*, D. C. Siegla and B. W. Smith, Plenum, New York, 1980, pp. 261–277.

[24]Neoh, K. G., "Soot Burnout in Flames," Ph.D. Dissertation, Dept. of Chemical Engineering, Massachusetts Inst. of Technology, Cambridge, MA, June 1980.

[25]Neoh, K. G., Howard, J. B., and Sarofim, A. F., "Effect of Oxidation on the Physical Structure of Soot," *Proceedings of the Combustion Institute*, Vol. 20, 1984, pp. 951–957.

[26]Garo, A., Lahaye, J., and Prado, G., "Mechanisms of Formation and Destruction of Soot Particles in a Laminar Methane-Air Diffusion Flame," *Proceedings of the Combustion Institute*, Vol. 21, 1986, pp. 1023–1031.

[27]Garo, A., Prado, G., and Lahaye, J., "Chemical Aspects of Soot Particles Oxidation in a Laminar Methane–Air Diffusion Flame," *Combustion and Flame*, Vol. 79, Nos. 3 and 4, 1990, pp. 226–233.

[28]Hardiquert, M., Cessou, A., Stepowski, D., and Coppalle, A., "OH and Soot Concentration Measurements in a High-Temperature Laminar Diffusion Flame," *Combustion and* Flame, Vol. 111, No. 4, 1997, pp. 338–349.

[29]Balthasar, M., Heyl, A., Mauss, F., Schmitt, F., and Bockhorn, H., "Flamelet Modeling of Soot Formation in Laminar Ethylene/Air Diffusion Flames," *Proceedings of the Combustion Institute*, Vol. 26, 1996, pp. 2369–2377.

[30]Bai, K. W., Balthasar, M., Mauss, F., and Fuchs, L., "Detailed Soot Modeling in Turbulent Jet Diffusion Flames," *Proceedings of the Combustion Institute*, Vol. 27, 1998, pp. 1623–1630.

[31]Mitchell, R. E., Sarofim, A. F., and Clomberg, L. A., "Experimental and Numerical Investigation of Confined Laminar Diffusion Flames," *Combustion and Flame*, Vol. 37, No. 3, 1980, pp. 227–244.

[32]Santoro, R. J., Semerjian, H. B., and Dobbins, R. A., "Soot Particle Measurements in Diffusion Flames," *Combustion and Flame*, Vol. 51, No. 2, 1983, pp. 203–218.

[33]Smyth, K. C., Miller, J. H., Dorfman, R. C., Mallard, W. G., and Santoro, R. J., "Soot Inception in a Methane/Air Diffusion Flame as Characterized by Detailed Species Profiles," *Combustion and Flame*, Vol. 62, No. 2, 1985, pp. 157–181.

[34]Santoro, R. J., Yeh, T. T., Horvath, J. J., and Semerjian, H. G., "The Transport and Growth of Soot Particles in Laminar Diffusion Flames," *Combustion Science and Technology*, Vol. 53, Nos. 2 and 3, 1987, pp. 89–115.

[35]Puri, R., Santoro, R. J., and Smyth, K. C., "The Oxidation of Soot and Carbon Monoxide in Hydrocarbon Diffusion Flames," *Combustion and Flame*, Vol. 97, No. 2, 1994, pp. 125–144.

[36]Puri, R., Santoro, R. J., and Smyth, K. C., "The Oxidation of Soot and Carbon Monoxide in Hydrocarbon Diffusion Flames," *Combustion and Flame*, Vol. 102, Nos. 1/2, 1995, pp. 226–228.

[37]Saito, K., Williams, F. A., and Gordon, A. S., "Structure of Laminar Coflow Methane–Air Diffusion Flames," *Journal of Heat Transfer*, Vol. 108, No. 3, 1986, pp. 640–648.

[38]McEnally, C. S., and Pfefferle, L. D., "Aromatic and Linear Hydrocarbon Concentration Measurements in a Non-Premixed Flame," *Combustion Science and Technology*, Vols. 115–117, Nos. 1–6, 1996, pp. 183–209.

[39]McEnally, C. S., and Pfefferle, L. D., "Flow Time Effects on Hydrocarbon Growth and Soot Formation in Coflowing Methane/Air Non-Premixed Flames," *Proceedings of the Combustion Institute*, Vol. 27, 1998, pp. 1539–1547.

[40]McEnally, C. S., Schaffer, A. M., Long, M. B., Pfefferle, L. D., Smooke, M. D., Colket, M. B., and Hall, R. J., "Computational and Experimental Study of Soot Formation in a Coflow Laminar Ethylene Diffusion Flame," *Proceedings of the Combustion Institute*, Vol. 27, 1998, pp. 1497–1505.

[41]Smooke, M. D., McEnally, C. S., Pfefferle, L. D., Hall, R. J., and Colket, M. B., "Computational and Experimental Study of Soot Formation on a Coflow, Laminar Diffusion Flame," *Combustion and Flame*, Vol. 117, Nos. 1/2, 1999, pp. 117–139.

[42]Dalzell, W. H., and Sarofim, A. F., "Optical Constants of Soot and Their Application to Heat Flux Calculations," *Journal of Heat Transfer*, Vol. 91, No. 1, 1969, pp. 100–104.

[43]Krishnan, S. S., Lin, K.-C., and Faeth, G. M., "Optical Properties in the Visible of Overfire Soot in Large Buoyant Turbulent Diffusion Flames," *Journal of Heat Transfer*, Vol. 122, No. 3, 2000, pp. 517–524.

[44]Chase, M. W., Jr., Davies, C. A., Downey, J. R., Jr., Frurip, D. J., McDonald, R. A., and Syverud, A. N., *JANAF Thermochemical Tables*, 3rd ed., *Journal of Physical Chemistry Reference Data*, Vol. 14, Supplement No. 1, 1986, p. 1211.

[45]McBride, B. J., Reno, M. A., and Gordon, S., "CET93 and CETPC: An Interim Updated Version of the NASA Lewis Computer Program for Calculating Complex Chemical Equilibrium with Applications," NASA TM 4557, 1994.

[46]Hamins, A., Gordon, A. S., Saito, K., and Seshadri, K., "Acetone Impurity in Acetylene from Tanks," *Combustion Science and Technology*, Vol. 45, Nos. 5 and 6, 1986, pp. 309, 310.

[47]Colket, M. B., III, Seery, D. J., and Palmer, H. B., "The Pyrolysis of Acetylene Initiated by Acetone," *Combustion and Flame*, Vol. 75, Nos. 3 and 4, 1989, pp. 343–366.

[48]Colket, M. B., III, Seery, D. J., and Palmer, H. B., "On Impurity Effects in Acetylene Pyrolysis," *Combustion and Flame*, Vol. 84, Nos. 3 and 4, 1991, pp. 434–437.

[49]Lahaye, J., and Prado, G., "Morphology and Internal Structure of Soot and Carbon Blacks," *Particulate Carbon*, edited by D. C. Siegla and G. W. Smith, Plenum, New York, 1981, pp. 33–55.

[50]Garo, A., Lahaye, J., and Prado, G., "Mechanisms of Formation and Destruction of Soot Particles in a Laminar Methane–Air Diffusion Flame," *Proceedings of the Combustion Institute*, Vol. 21, 1986, pp. 1023–1031.

[51]Hess, W. M., and Herd, C. R., "Microstructure, Morphology and General Physical Properties," *Carbon Black*, edited by J.-B. Donoret, R. C. Bansal, and M.-J. Wang, Marcel Dekker, New York, 1993, pp. 89–173.

[52]Ishiguro, T., Takatori, Y., and Akihama, K., "Microstructure of Diesel Soot Particles Probed by Electron Microscopy: First Observations of Inner Core and Outer Shell," *Combustion and Flame*, Vol. 108, Nos. 1/2, 1997, pp. 231–234.

[53]Kent, J. H., and Wagner, H. G., "Why Do Diffusion Flames Emit Smoke?," *Combustion Science and Technology*, Vol. 41, No. 1, 1984, pp. 245–269.

[54]Kent, J. H., and Wagner, H. G., "Temperature and Fuel Effects in Sooting Diffusion Flames," *Proceedings of the Combustion Institute*, Vol. 20, 1984, pp. 1007–1015.

[55]Boedecker, L. R., and Dobbs, G. M., "Soot Distribution and CARS Temperature Measurements in Axisymmetric Laminar Diffusion Flames with Several Fuels," *Proceedings of the Combustion Institute*, Vol. 21, 1986, pp. 1097–1105.

[56]Boedecker, L. R., and Dobbs, G. M., "CARS Temperature Measurements in Sooting Laminar Diffusion Flames," *Combustion Science and Technology*, Vol. 46, Nos. 3–6, 1986, pp. 301–323.

[57]Tesner, P. A., "Formation of Dispersed Carbon by Thermal Decomposition of Hydrocarbons," *Proceedings of the Combustion Institute*, Vol. 7, 1958, pp. 546–556.

[58]Tesner, P. A., "Dispersed Carbon Formation by Acetylene Self-Combustion," *Proceedings of the Combustion Institute*, Vol. 8, 1960, pp. 627–633.

[59]Libby, P. A., and Blake, T. R., "Theoretical Study of Burning of Carbon Particles," *Combustion and Flame*, Vol. 36, No. 2, 1979, pp. 139–169.

[60]Libby, P. A., and Blake, T. R., "Burning of Carbon Particles in the Presence of Water Vapor," *Combustion and Flame*, Vol. 41, No. 2, 1981, pp. 123–147.

[61]Johnstone, J. F., Chen, C. Y., and Scott, D. S., "Kinetics of the Steam–Carbon Reaction in Porous Graphite," *Industrial Engineering Chemistry*, Vol. 44, No. 7, 1952, pp. 1564–1569.

[62]Bradley, D., Dixon-Lewis, G., El-Din Habik, S., and Mushi, E. M. J., "The Oxidation of Graphite Powder in Flame Reaction Zones," *Proceedings of the Combustion Institute*, Vol. 20, 1984, pp. 931–940.

J. P. Gore
Associate Editor